DOI: 10.2352/ISSN.2470-1173.2016.12.IMSE-262

Analog Current Mode Implementation of Global and Local Tone Mapping Algorithm for WDR Image Display

Peng Chen [a], Kartikeya Murari [b] and Orly Yadid-Pecht [a]; [a]Integrated Intelligent Sensors Laboratory, [b]Integrated Circuits and Optical Imaging Laboratory, Electrical and Computer Engineering Department, University of Calgary; Calgary, Canada

Abstract

Tone mapping algorithms have been utilized to adapt wide dynamic range (WDR) images to limited dynamic range (LDR) displays while still maintaining images' details. This work presents an analog current mode circuitry approach to realize a tone mapping algorithm that includes both global and local operations in the image array periphery. Compared with the other in-pixel analog implementations, this work can keep the best pixel pitch and fill factor performance of WDR image sensors. In addition, by using joint global and local tone mapping operators, details of the images are preserved and the contrast of the image is also enhanced when compared with other hardware implementations realizing only one of these operators. In this work, a novel WDR analog divider is designed and presented to handle the WDR input pixel value. The circuit, designed in a TSMC 0.35 μm complementary metal oxide semiconductor (CMOS) technology, was simulated with thirty WDR images in order to evaluate our implementation. Peak signal to noise ratio (PSNR) and structural similarity (SSIM) scores were calculated to evaluate the hardware simulation and compared to a software implementation in MATLAB.

1. Introduction

With recent improvements in wide dynamic range (WDR) image capture technology, WDR sensors are utilized in all kinds of applications such as surveillance, telescope, machine vision, etc. [1-2]. For example, in medicine and biology, WDR image capture in endoscopy can help doctors and researchers observe the inside of the body better and diagnose more accurately. WDR sensor application in wildlife monitoring can provide information about wildlife status in both light and shade habitats.

However, there is a critical discrepancy between the WDR captured image and the limited dynamic range (LDR) of displays such as liquid-crystal display (LCD) monitors and cell phone screens. Natural sceneries often have a WDR ratio that exceeds 100,000:1 [3]. Most display devices are LDR which is 8-bit. Due to this disparity, the details and contrast of the WDR image are lost. To overcome this challenge, tone mapping algorithms have been used to adapt the captured WDR image to the LDR display devices while still maintaining image details and contrast.

Tone mapping algorithms can be classified into two main categories. One is a global tone reproduction [4] which deals with all pixels in the same way. The advantages of the global tone reproduction are high speed and low computational complexity. However, because it does not take the effect of spatial location into account, it causes loss of some local contrast.

The other type of tone mapping algorithms is a local tone reproduction [3] which takes the pixel's neighborhoods into consideration. The output of a pixel is related to that of the surrounding pixels. Even though it keeps the local tone contrast, there are also some disadvantages for the local tone mapping algorithms, such as greater time consumption and more computations. Another shortcoming is that it may introduce artifacts.

Apart from the above two processes, joint global and local tone mapping algorithms which combine the advantages of both global and local tone reproductions has also been developed [5]. The tone mapping algorithm of Ofili et al. [6] is another example shown to have a superior tone mapped image quality performance when comparing with conventional tone mapping algorithms. The algorithm is as follows:

$$\begin{cases} y(p) = \alpha \times \dfrac{1-e^{-\frac{x(p)}{x_0(p)}}}{1-e^{-\frac{x_{max}}{x_0(p)}}} \\ x_0(p) = k \times \mu_x + \dfrac{(x*h)(p)}{2} \end{cases} \quad (1)$$

Where p is a pixel in a color image, $x(p)$ is the luminance value of pixel p, $y(p)$ is the resulting luminance value after doing the tone mapping algorithm. The transformation and restoration between the luminance value of a pixel and its RGB color values are realized in YUV color space. x_{max} and μ_x are the maximum and mean luminance value of the color image. The factor k is a coefficient between zero and one and need adjust according to different images. * indicates the convolution operation. h is a two-dimensional spatial filter.

Apart from the development of tone mapping algorithms, another concern is the hardware implementation of such algorithms. There are mainly two approaches. One is based on digital circuits. Ofili et al. implemented their tone mapping algorithm in a field-programmable gate array (FPGA) [7]. Popovic et al. realized a FPGA implementation of Drago's logarithmic tone mapping algorithm by using Taylor approximation [8]. The advantages of a digital approach are its fast processing speed and excellent computational accuracy.

Another approach is an analog implementation. With the demand for WDR imaging in portable devices such as cell phones, power consumption and chip area are critical parameters. In addition, the input data of an analog approach is cleaner because it does not go through an analog-to-digital convertor (ADC) which adds additional noise such as quantization noise. Furthermore, the analog circuit is easier to integrate with WDR sensors. For above reasons, in this work, we selected analog circuits to realize our tone mapping algorithm because of its low power consumption and low silicon area. Abbass et al. realized a novel mixed design of a tone mapping technique for WDR CMOS image sensor [9]. Vargas-Sierra et al. reported a 151 dB WDR CMOS image sensor chip architecture with tone mapping compression embedded in-pixel [10]. Sicard et al. described a CMOS WDR imager with an analog local adaptation [11]. All the above three analog

DOI: 10.2352/ISSN.2470-1173.2016.12.IMSE-262

implementations were realized with the tone mapping algorithm at the pixel level. However, in-pixel circuitry resulted in a poor pixel pitch and an undesirable reduction in the fill factor. This is at odds with the typical requirements of minimum pixel pitch and maximum fill factor for high spatial resolution and sensitivity. Our proposed computation was implemented in the peripheral circuitry, therefore, it can maintain a small pixel pitch and high fill factor of a WDR sensor.

Besides, the above three analog implementations realized either global or local tone mapping algorithm. In this paper, we present a current-mode analog approach to realize Ofili's joint global and local tone mapping algorithm which has a superior image quality performance [6]. The outline of this paper is as follows: the three by three convolution and WDR analog divider are described in Section 2 and 3. Section 4 describes the exponential function. Section 5 shows the simulation results of the whole system and finally, Section 6 concludes the paper.

2. Convolution function

The algorithm considers not only the pixel itself but its surroundings to take the local contrast into account by utilizing the convolution operation. In this work, we used the Gaussian smoothing filter as our spatial filter as follows.

$$\mathrm{h} = \frac{1}{16}\begin{bmatrix} 1 & 2 & 1 \\ 2 & 4 & 2 \\ 1 & 2 & 1 \end{bmatrix} \tag{2}$$

Fig. 1 shows the convolution processing in detail. P11, P12…P33 are the nine pixel inputs in a three by three image patch. P22 is the center pixel. $P22_{out}$ is the center output pixel after doing the convolution and is described as follows:

$$P22_{out} = \frac{1}{16}(P11 + 2 * P12 + P13 + 2 * P21 + 4 * P22 + 2 * P23 + P31 + 2 * P32 + P33) \tag{3}$$

From the above, we can see that there are three different ratios we need to realize. They are 1/4, 1/8 and 1/16. In our algorithm, there is another 1/2 coefficient before the convolution. So, the three ratios become 1/8, 1/16 and 1/32. To realize these ratios in analog circuit, we used current mirrors appropriate sizing of the transistors as shown in Fig. 2. The sum of these currents is described as follows:

$$I_{out} = \frac{(W/L)_{1b}}{(W/L)_{1a}} I_1 + \frac{(W/L)_{2b}}{(W/L)_{2a}} I_2 + \ldots + \frac{(W/L)_{nb}}{(W/L)_{na}} I_n \tag{4}$$

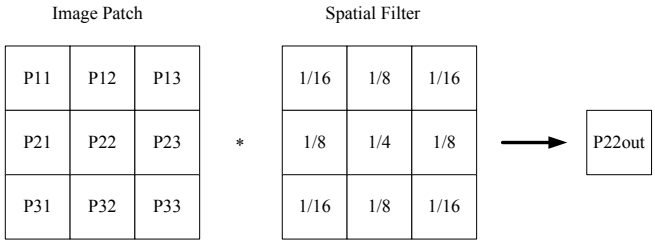

Figure 1. Three by three convolution processing

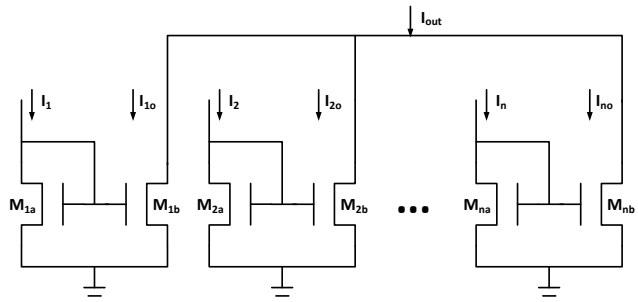

Figure 2.Current mirror circuit for convolution processing

3. WDR analog divider

The analog divider is the most difficult part in the implementation. Since both the numerator and denominator in the algorithm have a wide dynamic range of around 100 dB, it means that both numerator and denominator change over 5 orders of magnitude. In some mixed signal implementation of tone mapping algorithm, the authors utilized digital circuitry to do this kind of division [9]. However, this paper presents a novel way to solve this dynamic range problem purely in analog.

After testing several analog dividers, a current mode circuit which consists of geometric-mean cell and squaring cell was chosen as our basic core divider [12]. After simulation, we found that when the numerator and denominator changed from 10 μA to 100 μA, the division result was satisfactory. However, when they exceeded this range, the division error exceeded 20%, which is unacceptable.

The above analog divider was used as our basic core divider, and then adjustment and restoration circuits were added to let it handle the WDR inputs. After that, our WDR divider's error is less than 10% in the entire input range. By defining the maximum input current value as 100 μA, to reach the 100 dB dynamic range, the minimum input current value is 100 μA×10^{-5}=1 nA.

3.1. Adjustment circuit

Firstly, comparators were utilized to judge what the range of the original input value was. These four comparison results K1, K2, K3, K4 represented the range information of the numerator which is shown in (5) (6) (7) and (8). Another four comparison results KA, KB, KC, KD represented the range information of the denominator.

$$K1 = \begin{cases} 1 & \text{numerator} < 10nA \\ 0 & \text{numerator} > 10nA \end{cases} \tag{5}$$

$$K2 = \begin{cases} 1 & \text{numerator} < 100nA \\ 0 & \text{numerator} > 100nA \end{cases} \tag{6}$$

$$K3 = \begin{cases} 1 & \text{numerator} < 1uA \\ 0 & \text{numerator} > 1uA \end{cases} \tag{7}$$

$$K4 = \begin{cases} 1 & \text{numerator} < 10uA \\ 0 & \text{numerator} > 10uA \end{cases} \tag{8}$$

Secondly, range information K1, K2, K3, K4 was used to adjust the numerator's range into [10μA, 100μA] which is the working range of the basic core divider. The schematic of

©2016 Society for Imaging Science and Technology
DOI: 10.2352/ISSN.2470-1173.2016.12.IMSE-262

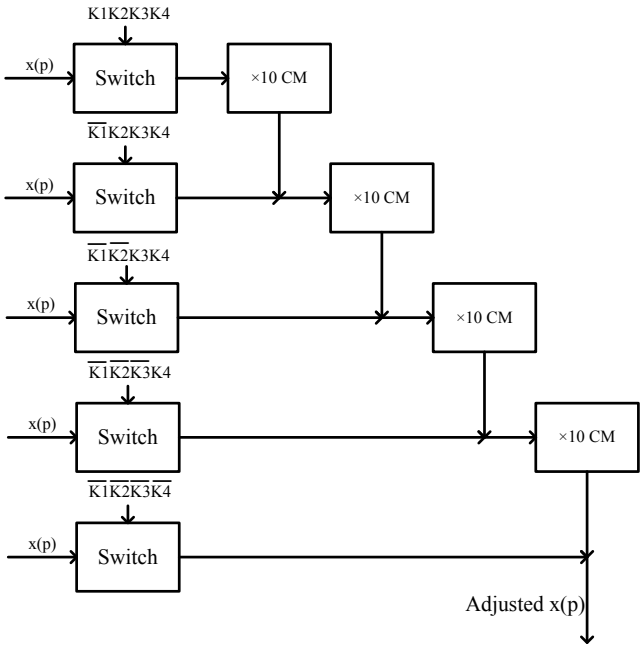

Figure 3. Schematic of adjustment circuitry for the numerator

adjustment circuitry of numerator $x(p)$ is shown in Fig.3. Switches and current mirrors were utilized to realize it.

The idea is that different numbers of ×10 current mirrors are utilized to adjust the current according to its range information. For example, if the input is 5 nA, only the first row's switch is on which means that only the first row's input current flows through all four ×10 current mirrors. So the input is enlarged by 10^4 times. The adjusted value is 50 μA which is in the working range of the basic core divider. By using these judgement and adjustment circuitries for both WDR numerator and denominator, they are adjusted to the working range of the basic core divider with their associated range information.

3.2. Restoration circuit

After the processing of the adjustment circuitry, the adjusted numerator and denominator were applied into the basic core divider to do the division. A restoration operation was added to restore the correct division result. We use R' to present the adjusted division result and R to present the correct division result. The processing details can be seen in Table I. N represents the numerator and D represents the denominator. Every blank part in the table means that this division situation is impossible in practice according to the algorithm's mathematical properties. In the algorithm, for the division $(-\frac{x(p)}{x_{0(p)}})$ in (1), we can see that the denominator $x_0(p)$ is always larger than $\frac{1}{8}\times x(p)$ because the property of the three by three Gaussian filter. For the second division $(-\frac{x_{max}}{x_{0(p)}})$ in (1), x_{max} is 100 μA, and we can directly assume this exponent term $(e^{-\frac{x_{max}}{x_{0(p)}}})$ equals to zero when $x_0(p)$ is less than 5 μA. Therefore, those blank parts are impossible in practice.

By following the idea of table I, the restoration circuitry was designed by comparators and current mirrors; controlled by the range information K1, K2, K3, K4 and KA, KB, KC, KD. The

Table I. Restoration of division results

R / N	D	[1nA, 10nA]	[10nA, 100nA]	[100nA ,1μA]	[1μA, 10μA]	[10μA, 100μA]
[1nA, 10nA]		R'	0.1*R'	0.01*R'	0.001* R'	0.0001 *R'
[10nA, 100nA]		10*R'	R'	0.1*R'	0.01*R'	0.001* R'
[100nA ,1μA]		100*R'	10*R'	R'	0.1*R'	0.01*R'
[1μA, 10μA]			100*R'	10*R'	R'	0.1*R'
[10μA, 100μA]				100*R'	10*R'	R'

circuit's structure was very similar with the adjustment circuit, so the specific circuit is not shown in this paper.

4. Exponential function

A MOS transistor in sub-threshold region was used to realize the exponential function. When the transistor works in the sub-threshold region, Id is described as follows:

$$I_D = \frac{W}{L} I_t \exp\left(\frac{V_{GS}-V_{th}}{nV_T}\right)[1-\exp(-\frac{V_{DS}}{V_T})] \quad (9)$$

$$I_t = qXD_n n_{p0} \exp\left(\frac{\Psi_S}{V_T}\right) \quad (10)$$

W and L are the width, length of the transistor and X is the thickness of the cross-sectional area in which the diffusion current flows. V_{DS}, V_{GS} and V_{th} are the drain-source, gate-source and threshold voltage. V_T is the thermal voltage and q is the unit charge. D_n is the diffusion constant for electrons. n_{p0} is the equilibrium concentration of electrons in the substrate. Ψ_S is the surface potential. All the parameters in (10) are constant once the CMOS technology is fixed. In addition, the last term $\exp(-\frac{V_{DS}}{V_T})$ in (9) approximately equals to zero, when Vds > $3V_T$.Therefore, the drain current I_D can be controlled by the term $(V_{GS}-V_{th})$ under the exponential function [13].

5. Simulation results

To evaluate the performance of our hardware implementation, thirty different WDR images from our database were tested and simulated by our transistor-level design in Cadence. For comparing visual quality, five groups of WDR images including the original WDR images, output images from the hardware implementation and output images from a MATLAB software implementation are shown in Fig.4. The comparison results show that there are almost no visual differences between the hardware simulation images and the software simulation images.

To compare the two tone-mapped images quantitatively, the peak signal to noise ratio (PSNR) and structural similarity (SSIM) were calculated by (11) (12). For PSNR in (11), I(m,n) is the ideal software result value for the pixel in row m and column n. T(m,n)

DOI: 10.2352/ISSN.2470-1173.2016.12.IMSE-262

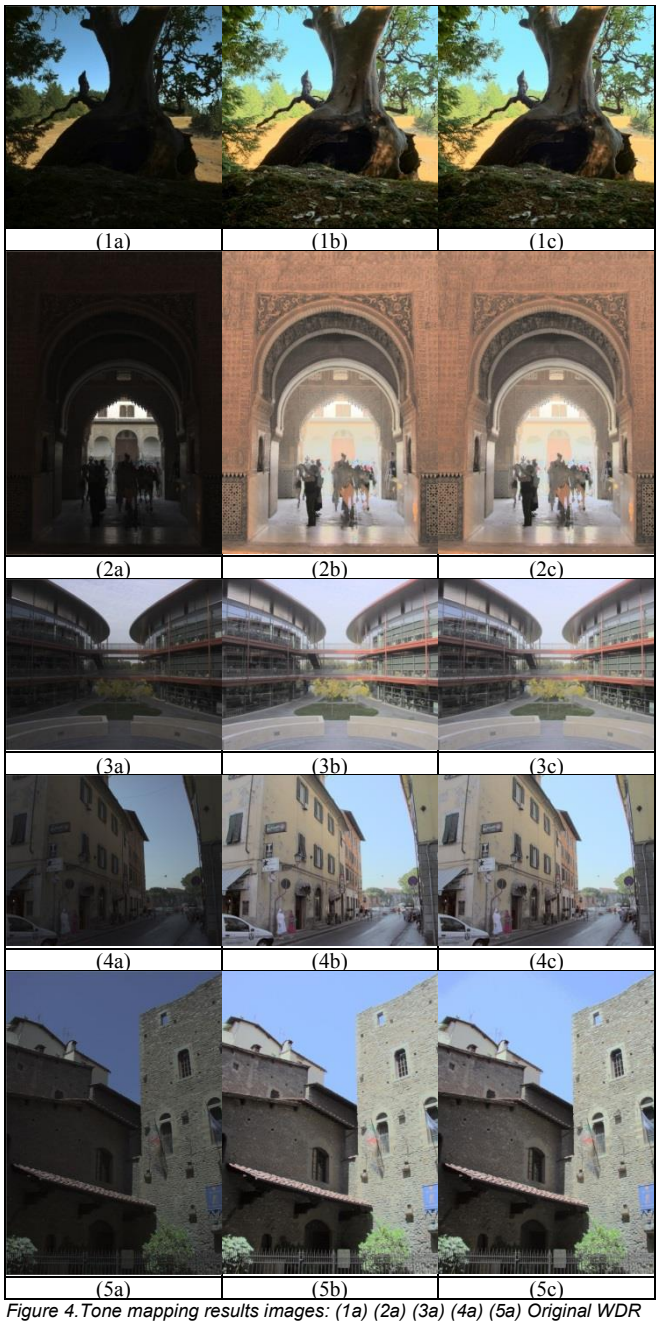

Figure 4.Tone mapping results images: (1a) (2a) (3a) (4a) (5a) Original WDR images (1b) (2b) (3b) (4b) (5b) Tone mapped images by the software simulation (1c) (2c) (3c) (4c) (5c) Tone mapped images by the hardware simulation

is the hardware simulation result value for that pixel [7]. 255 is the maximum value for an 8-bit LDR display. Higher PSNR values represent that objective image quality is better.

$$\text{PSNR} = 10 \times log_{10}[\frac{255^2}{\frac{1}{MN}\sum_{m=1}^{M}\sum_{n=1}^{N}[I(m,n)-T(m,n)]^2}] \quad (11)$$

For SSIM in (12), μ_x and μ_y are the mean value of image x and y. σ_x and σ_y are the variance of x and y. The covariance of x and y is presented by σ_{xy}. C_1 and C_2 are two constants to prevent instability in the division which are $(255 \times 0.1)^2$ and $(255 \times 0.3)^2$ [14]. The structural similarity between two images is better when the SSIM gets closer to one.

$$\text{SSIM} = \frac{(2\mu_x\mu_y+C_1)(2\sigma_{xy}+C_2)}{(\mu_x{}^2+\mu_y{}^2+C_1)(\sigma_x{}^2+\sigma_y{}^2+C_2)} \quad (12)$$

Table II. PSNR and SSIM results

	No. 1	No. 2	No. 3	No. 4	No. 5	Average of thirty images
PSNR	35.32 dB	34.33 dB	36.74 dB	36.32 dB	33.16 dB	34.45 dB
SSIM	0.990	0.989	0.993	0.994	0.986	0.987

The PSNR and SSIM measurement results are shown in Table II. The results show that the differences in images are very small and that the structural similarity between them is very good.

According to the simulation result in Cadence, this analog current mode implementation consumed an area of 0.039 mm^2 and a static power of 41 mW from a 3.3 V supply under TSMC cmosp35 technology. The area was approximated by summing up the product of width and length for all transistors. The processing time was 1 µs for each pixel. Because the power and area are small when comparing with other digital hardware implementations [7], repeated circuits in parallel can be utilized for increasing the speed if the customer needs.

6. Conclusion

In this paper, we have presented an analog current-mode approach to realize the joint global and local tone mapping algorithm of Ofili et al. [6]. A novel WDR analog divider is presented to handle the WDR input values. And the resulting simulation images are shown in LDR display with high contrast and good detail performance. This implementation is a good choice for the real-time low-power applications especially for the portable devices because of its low-power and low-area properties.

Acknowledgment

This work is supported by CMC for Cadence. Authors thank Dr. A. Spivak, Dr. A. Horé and the lab mates for consultation and advice. Dr. O. Yadid-Pecht and Dr. K. Muarari are supported by iCORE/AITF.P. Chen is supported by NSERC and iCORE/AITF.

References

[1] Y. Dattner, and O. Yadid-Pecht, "High and Low Light CMOS Imager Employing Wide Dynamic Range Expansion and Low Noise Readout," Sensors Journal, vol. 12, issue. 6, pp. 2172–2179, 2012.

[2] A. Belenky, A. Fish, A. Spivak, and O. Yadid-Pecht, "Global shutter CMOS image sensor with wide dynamic range," Circuits and Systems II: Express Briefs, vol. 54, issue. 12, pp. 1032–1036, 2007.

[3] J. Duan, W. Dong, R. Mu, G. Qiu, and M. Chen, "Local contrast stretch based tone mapping for high dynamic range images," Computational Intelligence for Multimedia, Signal and Vision Processing (CIMSIVP), pp. 26–32, 2011.

DOI: 10.2352/ISSN.2470-1173.2016.12.IMSE-262

[4] F. Drago, K. Myszkowski, T. Annen, and N. Chiba, “Adaptive logarithmic mapping for displaying high contrast scenes,” Computer Graphics Forum, vol. 22, issue.3, pp. 419-426, 2003.

[5] A. Hore, and O. Yadid-Pecht, “A statistical derivation of an automatic tone mapping algorithm for wide dynamic range display,” Acoustics, Speech and Signal Processing (ICASSP), pp. 2475–2479, 2014.

[6] C. Ofili, S. Glozman, and O. Yadid-Pecht, “An in-depth analysis and image quality assessment of an exponent-based tone mapping algorithm,” International Journal Information Models and Analysis, vol. 1, pp. 236–250, 2012.

[7] C. Ofili, S. Glozman, and O. Yadid-Pecht,“Hardware implementation of an automatic rendering tone mapping algorithm for a wide dynamic range display,” Low Power Electronics and Applications, vol. 3, pp. 337-367, 2013.

[8] V. Popovic, E. Pignat, and Y. Leblebici, “Performance Optimization and FPGA Implementation of Real-Time Tone Mapping,” Circuits and Systems II: Express Briefs, IEEE Transactions on, vol.61, issue. 10, pp. 803-807, 2014

[9] H. Abbass, H. Amhaz, G. Sicard, and D. Alleysson “Novel Mixed Design of Tone Mapping Technique for HDR CMOS Image Sensor,” 25th IEEE International Conference on Microelectronics (ICM), pp. 1-4, 2013.

[10] S. Vargas-Sierra, G. Liñán-Cembrano, and A. Rodríguez-Vázquez, “A 151dB High Dynamic Range CMOS Image Sensor Chip Architecture with Tone Mapping Compression Embedded in-Pixel,” Sensors Journal, IEEE, vol. 15, issue. 1, pp. 180-195, 2015.

[11] G. Sicard,H. Abbas, H. Amhaz, H. Zimouche, R. Rolland, and D. Alleysson, “A CMOS HDR Imager with an Analog Local Adaptation,” International Image Sensor Workshop, pp. 1-4, 2013.

[12] A. López-Martín, and A. Carlosena, “Current-mode multiplier/divider circuits based on the MOS translinear principle,” Analog Integrated Circuits and Signal Processing, vol. 28, issue. 3, pp. 265-278, 2001.

[13] P. Gray, P. Hurst, S. Lewis, and R. Meyer, “Analysis and design of analog integrated circuits”, pp. 65-67, 5th edition, John Wiley & Sons, Inc., 1990.

[14] Z. Wang, A. C. Bovik, H. R. Sheikh, and E. P. Simoncelli, "Image quality assessment: From error visibility to structural similarity," IEEE Transactions on Image Processing, vol. 13, issue. 4, pp. 600-612, Apr. 2004.

Author Biography

Peng Chen received his B.Sc degree in electronics science and technology from Nanjing University of Aeronautics and Astronautics, Nanjing, China in 2013. Currently, he is working towards the M.Sc degree in electrical and computer engineering at University of Calgary, Calgary, Canada, as a research assistant. His research interests include analog/mixed VLSI design and image processing.

Kartikeya Murari has a B.Tech. (2002) in electrical engineering from the Indian Institute of Technology Madras, and MSE (2004) and PhD (2010) degrees in biomedical engineering from the Johns Hopkins University, where he also trained as a postdoctoral fellow till 2012. Currently, he is an Assistant Professor in the Department of Electrical and Computer Engineering at the University of Calgary. His research interests lie in electronic and optical techniques and instrumentation for studying the brain.

Orly Yadid-Pecht received her D.Sc. from the Electrical Engineering Department at the Technion—Israel Institute of Technology in 1995. She was a National Research Council (USA) research fellow from 1995–1997 in the areas of Advanced Image Sensors at the Jet Propulsion Laboratory (JPL)/California Institute of Technology (Caltech). In 1997, she joined Ben-Gurion University in Israel, as a member in the Electrical and Electro-Optical Engineering departments.There she founded the VLSI Systems Center, specializing in CMOS image sensors. Since 2009, she is the iCORE Chair of Integrated Intelligent Sensing Laboratory (I2Sense, formerly ISIS) at the University of Calgary, Canada. Dr. Yadid-Pecht’s main subject of interest is Integrated CMOS Sensors. She is interested in compact low-power micro- and nano-systems mainly for biomedical applications (but not exclusively). She has published over a hundred papers, holds more than two dozen patents, and has led over two dozen research projects supported by government and industry. In addition, she has coauthored and co-edited the first book on CMOS Image Sensors: ‘‘CMOS Imaging: From Photo-transduction to Image Processing,’’ published in 2004. Dr. Yadid-Pecht is also a director on the board of two companies, and she is an IEEE and SPIE Fellow.